



Project funded by the European Commission under the 6th (EC) RTD Framework Programme (2002- 2006) within the framework of the specific research and technological development programme "Integrating and strengthening the European Research Area"



## Project UpWind

Contract No.:  
019945 (SES6)

"Integrated Wind Turbine Design"



---

## WP6: Remote Sensing

### D6.6.2 Measurements in complex terrain using a lidar

---

AUTHOR:	Paula Gómez Arranz
AFFILIATION:	Fundación CENER-Ciemat
ADDRESS:	C/ Ciudad de la Innovación. 31621 Sarriguren. Navarra. Spain
TEL.:	+34 948 25 28 00
EMAIL:	<a href="mailto:pgomez@cener.com">pgomez@cener.com</a>
FURTHER AUTHORS:	
REVIEWER:	
APPROVER:	

#### Document Information

DOCUMENT TYPE	Final Report
DOCUMENT NAME:	CENER-D6.6.2-final.pdf
REVISION:	
REV.DATE:	February 2011
CLASSIFICATION:	R0: General public
STATUS:	

**Abstract:** This document presents the results of a measurement campaign in complex terrain performed by CENER using a lidar and an instrumented met mast in front of a wind turbine.

---

## Contents

---

1.	Introduction .....	4
2.	Description of the test site .....	4
3.	Meteorological mast instrumentation and lidar configuration .....	7
3.1	Description of meteorological mast and sensors .....	7
3.2	Specifications of the mast sensors .....	9
3.3	Free sectors .....	9
3.4	Cup anemometer uncertainty .....	9
3.5	ZephIR configuration .....	9
3.6	Data acquisition systems .....	10
4.	Data Filters .....	10
4.1	Filter #1: mast sensors .....	10
4.2	Filter #2: lidar “PiF” and “PiA” .....	11
4.3	Filter #3: Cloud/Fog .....	12
4.4	Filter #4: “Turbulence” parameter .....	14
4.5	Availability of mast and lidar data .....	15
4.6	Availability and reliability of ZephIR .....	15
5.	Analysis of Results .....	17
5.1.1	Mean horizontal wind speed analysis .....	17
5.1.2	Wind direction analysis .....	26
5.1.3	Vertical wind speed analysis – Rain influence .....	27
5.1.4	Wind flow angle analysis .....	28
5.1.5	Turbulence analysis .....	30
6.	Modelling lidar measurements .....	32
6.1	Wasp Engineering lidar Script .....	33
6.2	CFD modelling .....	33
6.2.1	Description of CFDWind 2.0 .....	33
6.2.2	Set-up .....	34
6.3	Results .....	34
7.	Conclusions .....	35
8.	Acknowledgements .....	36
9.	References .....	36

STATUS, CONFIDENTIALITY AND ACCESSIBILITY							
Status			Confidentiality			Accessibility	
<b>S0</b>	Approved/Released		<b>R0</b>	General public	x	Private web site	
<b>S1</b>	Reviewed		<b>R1</b>	Restricted to project members		Public web site	
<b>S2</b>	Pending for review		<b>R2</b>	Restricted to European. Commission		Paper copy	
<b>S3</b>	Draft for comments		<b>R3</b>	Restricted to WP members + PL			
<b>S4</b>	Under preparation		<b>R4</b>	Restricted to Task members +WPL+PL			

**PL:** *Project leader*    **WPL:** *Work package leader*    **TL:** *Task leader*

## 1. Introduction

CENER's contribution to work package 6, task 6.6, consists of a measurement campaign in complex terrain, in which a ZephIR lidar is installed close to a meteorological mast and in the vicinity of a wind turbine. The aim is to perform comparisons between the lidar and the meteorological mast instrumentation, in order to enhance the knowledge on lidar behaviour in complex terrain, and to identify the problems and limitations that remote sensing may suffer in this situation, as well as sources of bias or error. Simultaneous to this lidar to mast correlation study, the power curve measurement of the nearby wind turbine is carried out. In a separate deliverable D6.15.1 [1], the results of the power curve measurement with lidar, to which task 6.15 is dedicated, are presented.

The measurement campaign started in August 2008, after some delay from the original start-up date (initially, march 2008), due to delays in the development and grid connection of the wind farm where the campaign takes place. The measurement campaign was interrupted in October 2008 due to a lidar failure (damage of the laser), and the instrument was sent to Natural Power for replacement of the laser unit, a general maintenance service, as well as an upgrade to the latest system specifications at that moment. After the return of the repaired lidar, the campaign was resumed in February 2009. The measurement campaign was finished in September 2009.

The results of the first part of the campaign (August 2008 to October 2008; prior to lidar failure) were presented in the 30-month progress report. Some preliminary results of the second phase of the campaign were presented in CENER's summaries of activities in months 36 and 42. This document is the final report corresponding to task 6.6.

## 2. Description of the test site

The test site is a wind farm in complex terrain, located in Albacete, Spain. The test area consists of hills covered with forest, and several rows of wind turbines, as seen in Figure 1. The terrain is fairly irregular in all directions (Figure 2).



**Figure 1:** *Wind farm view*

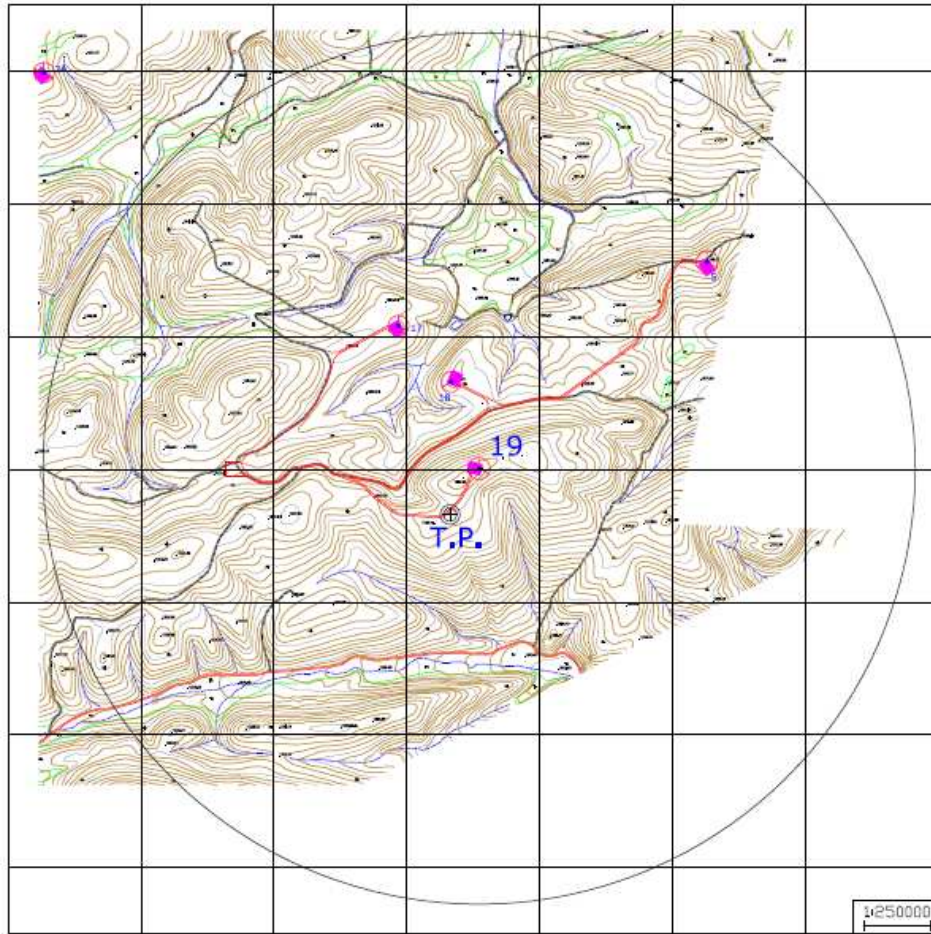


**Figure 2:** 5m-contour-line map with a general view of the area. Mast and lidar position is labelled "T.P." Altitude in that point is 1300m.

The lidar (ZephIR) is installed close to a meteorological mast (equipped with cup anemometers, wind vanes, vertical propeller anemometer and sonic anemometers) and in the vicinity of a wind turbine. In an attempt to maximize the correlation between lidar and mast measurements, the ZephIR is located as close as possible to the mast, but not too close in order to avoid the mast blocking a significant amount of the laser beams. The lidar is deployed at 12m distance from the mast, in the SW direction. The closest wind turbine is 205m away from the mast, in the N-NE direction. Prevailing wind direction is West, and the secondary is South.

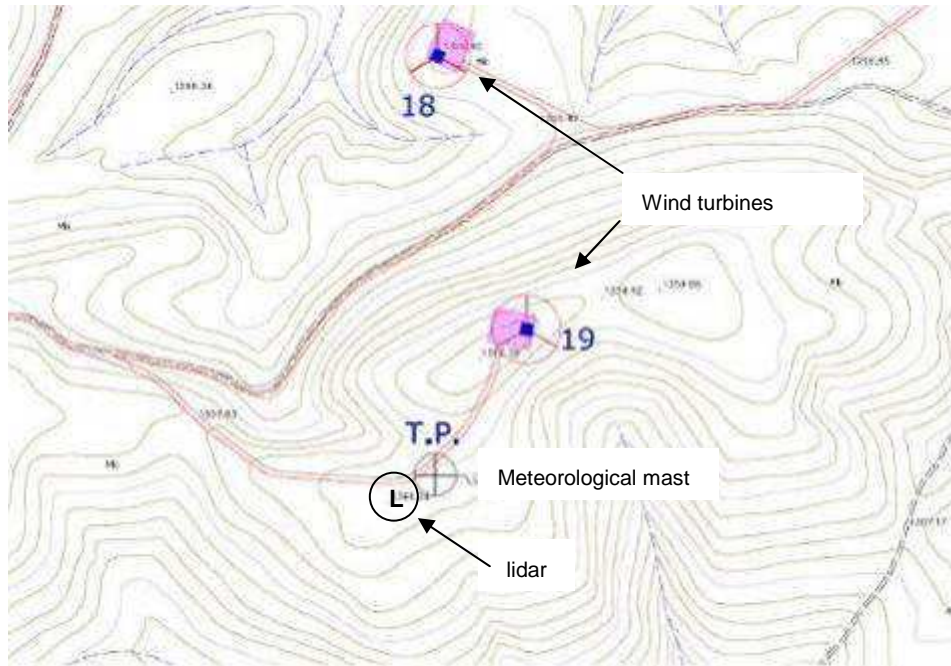


**Figure 3:** Close-up of the area where the lidar is deployed.



**Figure 4:** Position of lidar relative to mast and wind turbine.



**Figure 5:** Location of meteorological mast, lidar and nearest wind turbine. Picture is taken from the West.

### 3. Meteorological mast instrumentation and lidar configuration

#### 3.1 Description of meteorological mast and sensors

The meteorological mast is 79m high, and has cup anemometers, vanes and sonic anemometers at different levels, to which lidar measurements (wind speeds and wind directions) are compared. The mast is equipped with additional meteorological sensors such as pressure and temperature, as detailed in Table 1.

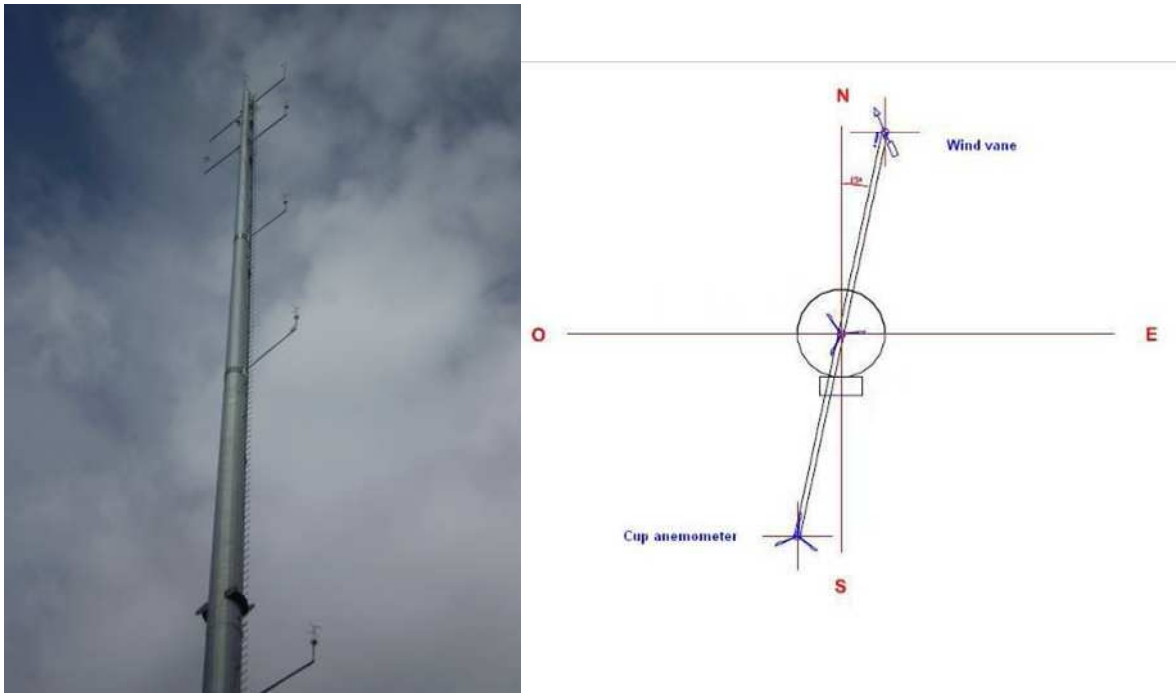


**Figure 6:** Image of the meteorological mast (left) and scheme plan view (right)

The mast was originally designed for power curve verification purposes, and was erected with the instrumentation required by the standard and following the mounting arrangement recommendations of [2, Annex G] in the top levels (79m to 74m). Afterwards, and for the purpose of this UpWind campaign, four sonic anemometers were added to the mast, mounted on booms of length increasing with mast width, in order to alleviate flow distortion caused by the mast.

There is a top-mounted cup anemometer. The rest of the cup anemometers, the vanes, and the sonic anemometers are mounted on booms, with orientations of either  $15^\circ$  or  $195^\circ$  with respect to North (perpendicular to the prevailing wind direction), as can be seen in Figure 6. Sensor heights and boom orientations are detailed in Table 1.

Sensor	Height a.g.l. (m)	Boom orientation
Cup anemometer	79	-
Cup anemometer	77	$195^\circ$
Wind Vane	77	$15^\circ$
Propeller	74	$15^\circ$
Sonic anemometer	74	$195^\circ$
Humidity & Temperature sensor	74	-
Sonic anemometer	66	$195^\circ$
Sonic anemometer	58	$195^\circ$
Sonic anemometer	43	$195^\circ$
Cup anemometer	40	$195^\circ$
Wind Vane	40	$15^\circ$
Pressure sensor	1.5	-
Rain sensor	1.5	-

**Table 1:** Meteorological mast instrumentation.

### 3.2 Specifications of the mast sensors

All sensors of the same type are from the same manufacturer and of the same model. Sensor models are specified in Table 2.

Type of Sensor	Model
Cup anemometer	Thies First Class
Wind Vane	Thies-Compact
Propeller	Young 27106T-Y
Sonic anemometer	Metek USA-1 Basic
Humidity & Temperature sensor	Ammonit –P6831
Pressure sensor	Vaisala-PTB100A
Rain sensor	Lambrecht

**Table 2:** Meteorological mast sensor models

The pressure sensor, temperature and humidity sensor, and the propeller have been calibrated by laboratories accredited by UNE-EN ISO/IEC 17025 standard [3]. Additionally, cup anemometers have been calibrated by a laboratory accredited by Measnet [4]. The sonic anemometers are configured with their individual factory calibration parameters [5].

### 3.3 Free sectors

In order to ensure that the measurements of meteorological mast sensors are not influenced by wakes from the neighbouring wind turbines, an assessment of obstacles is carried out according to [2, annex A]. Apart from the wind farm's wind turbines, there aren't other significant obstacles in the area. The free sector has been found to be [75°,325°).

### 3.4 Cup anemometer uncertainty

The cup anemometer with the lowest uncertainty is the one at 79m since it is top mounted. For this reason it will be used as the wind speed reference to which lidar wind speed will be compared to in many parts of this report. Its uncertainty can be expressed as [2]:

$$u_v = \sqrt{u_{v1}^2 + u_{v2}^2}$$

Where:

- $u_{v1}$  is the uncertainty in the anemometer calibration.  $u_{v1}=0.08\text{m/s}$
- $u_{v2}$  is the uncertainty due to the operational characteristics of the anemometer,  
 $u_{v2} = (0.05\text{m/s} + 0.005 \cdot U) \cdot k / \sqrt{3}$   
 where U is the wind speed and k is the class of the anemometer (k=2.9)

The uncertainties due to mounting effects and acquisition system can be neglected in this case.

### 3.5 ZephIR configuration

The ZephIR is configured to measure at heights 40, 58, 66 and 79m above ground level, matching the heights of the mast sensors relevant to this study, and to which lidar measurements are compared. An additional height of 100m is configured in order to obtain lidar wind data above mast height. Two additional heights are sensed (as a factory setting), 38m and 800, which are used only by the ZephIR internal cloud correction software to process wind data in order to compensate for cloud effects. The version of the cloud correction algorithm was the

latest developed up to that date, and it is the one described in [7]. Scan settings are modified from the factory default three-second scan per height [8] to one-second scan per height.

### 3.6 Data acquisition systems

All the instruments in the mast, except the sonics, are sampled at a frequency of 1Hz and their 10-minute statistics are stored in a datalogger. The sonics are sampled at 20Hz and their data is stored in a pc and post-processed to 10-minute period statistics.

1-second ZephIR data is stored in its internal memory card. A backup of its raw data is streamed to the computer during some periods of the campaign.

Each of the three acquisition systems (ZephIR, computer and datalogger) is provided with a GSM modem that allows for data transmission and remote supervision of the equipment. Time synchronization of the three systems is achieved by a remote computer.

## 4. Data Filters

All datasets are processed to 10-minute period statistics. A common database is created from data recorded from 24/2/2009 14:10 to 3/8/2009 16:20. This database consists of simultaneous ten-minute values of mast and lidar data.

Interruptions of the acquisition of sonic data happened during different periods in this campaign due to failure of the computer used for data storage and processing. Also, lidar "9999" wind speed readings (an indication of lack of wind speed measurement due to low aerosol concentration) are not included in this database. However, they will be taken into account in the lidar availability calculation of section 4.6.

A selection of filters has been applied to mast and lidar data in order to ensure the quality of the dataset. The used filters are described in this section, where it is presented the consecutive application of each of them. Their effect on data availability is presented in 4.5.

As a way to evaluate the filter's effectiveness, the lidar wind speed is compared to cup wind speed at 79m.

For the sake of confidentiality, and as a request from the wind farm owner, the following graphs as well as the majority of the graphs included in this report are presented in dimensionless units. This means that some wind measurements (such as speeds or wind flow angles, etc) are divided by either one constant reference value of wind speed ( $U_{REF}$ ) or by one constant reference angle ( $\theta_{REF}$ ).

### 4.1 Filter #1: mast sensors

Mast data are filtered out from the database according to the following criteria:

- Damage or incorrect functioning of the equipment due to: supply failure, freezing (Temperature  $\leq 2^{\circ}\text{C}$ ), broken sensor, failure of the acquisition system, etc.
- Wind direction from a perturbed sector, either due to wakes from neighbouring wind turbines, or by mast mounting effects. For the top-mounted cup, the non-perturbed sector is  $[75^{\circ}, 325^{\circ})$ . For the boom-mounted sensors, the non-perturbed sectors are considered to be  $[85^{\circ}, 125^{\circ})$  and  $[265^{\circ}, 305^{\circ})$ ; that is,  $\pm 20^{\circ}$  wind direction sectors with centres  $90^{\circ}$  to the boom.

- Wind speeds out of the range [4,16) m/s, which is the calibration range of the cup anemometers.

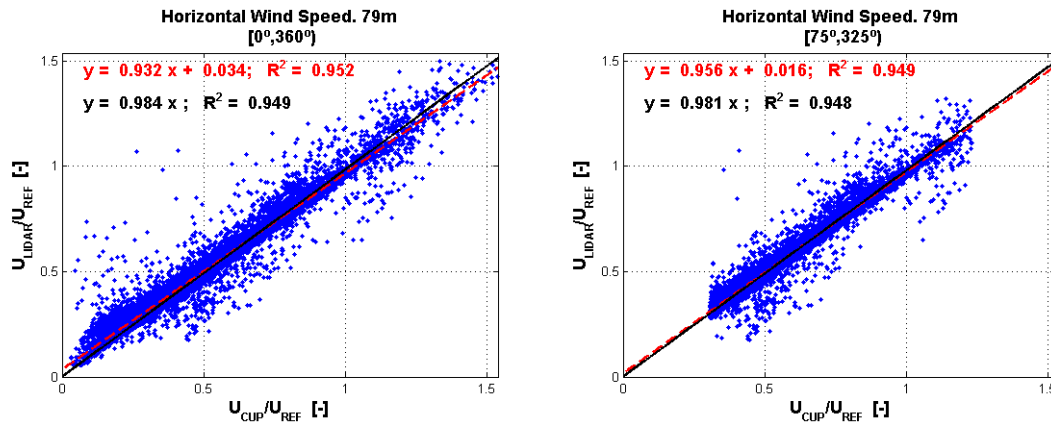


**Figure 7:** Left: lidar to cup wind speed comparison obtained from the total (unfiltered) dataset. Right: Result of applying mast data filters (Filter #1).

## 4.2 Filter #2: lidar “PiF” and “PiA”

The most basic filtering to be applied to lidar data is to impose two conditions:

- There are a minimum number of radial wind speed measurements per scan, from which the instantaneous wind vector at that height is derived [8].
- There is a minimum number of instantaneous wind speed data (“one-second data”) in each ten-minute period, per height.

Those two parameters are respectively called “Points in Fit” (PiF) and “Packets in Average” (PiA) and are provided by ZephIR. The lidar output files, which consist of ten-minute average values of wind measurements as well as other parameters, include the average number of Points in Fit per 10-minute record, and the number of data recorded in each ten minute interval, per height.

The following limits have been chosen for the filtering:  $PiF \geq 35$  <sup>(1)</sup> and  $PiA \geq 50$ .

Figure 8 shows the effect of applying simultaneously filter#1 and filter#2. Significant negative and positive errors are observed in the lidar wind speed measurements. In 4.3 we investigate the dependence of such differences to the presence of clouds and fog.

<sup>1</sup> Note that since the ZephIR is working in a one-second-scan configuration, the maximum value of PiF is 50

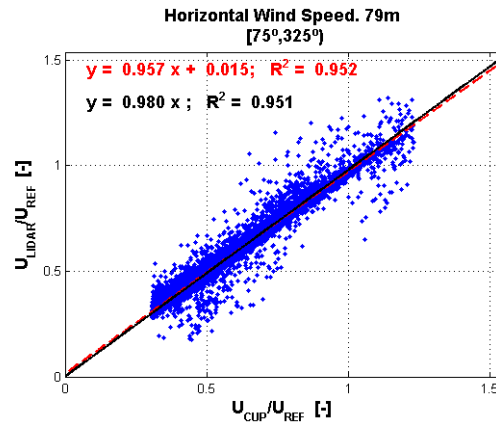


**Figure 8:** Lidar to cup wind speed regression obtained by applying mast filters (filter#1) and lidar PiF and PiA filters (filter#2).

### 4.3 Filter #3: Cloud/Fog

During the process followed by the ZephIR's internal cloud correction algorithm to detect the presence of clouds and correct radial wind speed measurements in order to remove cloud contamination, a certain set of parameters are used. They are:

- The Scaling value of the Doppler spectra at 38m ( $S_{38}$ )
- The Scaling value of the Doppler spectra at 800m ( $S_{800}$ )
- The Scaling Ratio ( $SR = S_{38} / S_{800}$ )
- The Cloud Scaling parameter

The meaning of each of these parameters and their role in the cloud correction procedure is described in [7]. The 10-minute average values of these parameters are output in the ZephIR data files. In Figure 9 and Figure 10 the wind speed difference ( $U_{LIDAR} - U_{CUP}$ ) is plotted versus the four of them.

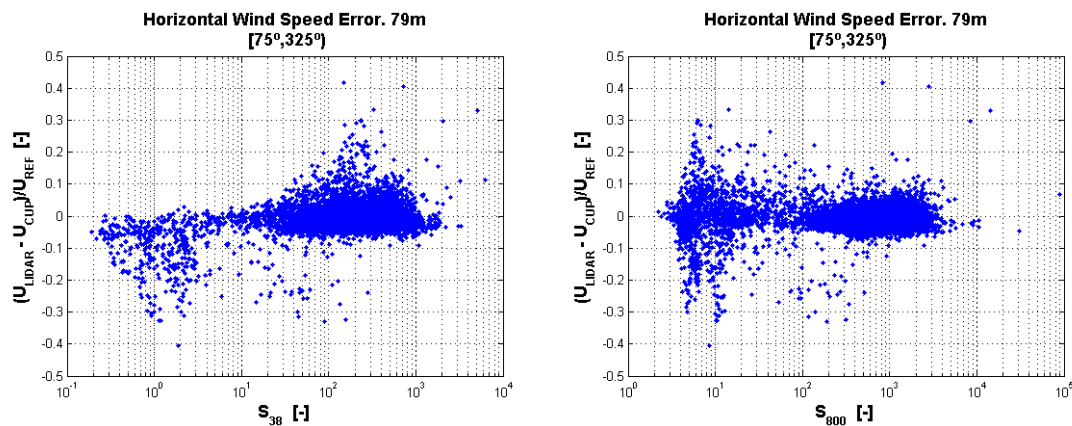


**Figure 9:** Lidar error vs Scaling value at 38m,  $S_{38}$  (left) and Lidar error vs Scaling value at 800m,  $S_{800}$  (right).

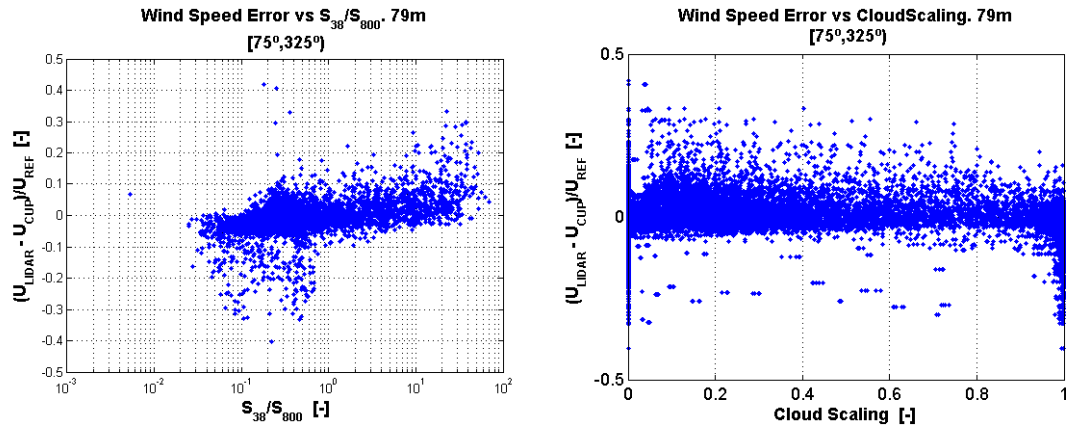


**Figure 10:** Left: Lidar error vs Scaling Ratio ( $S_{38}/S_{800}$ ). Right: Lidar error vs “cloud scaling” parameter at 79m.

In Figure 9 and Figure 10, two situations are observed:

- Case 1: Big negative errors appear for values of  $S_{38} < 10$ ,  $S_{800} < 25$ , and  $SR < 0.1$
- Case 2: Big positive errors appear for values of  $S_{800} < 25$ , and  $SR > 10$ .

In case 1:

- A low value of  $S_{38}$  means high (averaged) amplitude of the spectral peak at 38m, that is: strong backscatter from 38m height. That would indicate a cloud layer (fog) in that height or below. In a similar way, a low value of  $S_{800}$  indicates that the collimated laser beam is strongly backscatter by a cloud layer.
- Under fog conditions, low values of  $S_{38}$  and  $S_{800}$  can be expected.
- In such case (fog), the big negative error in the wind speed measurement at 79m might be explained in this way:
  - For all measurement heights (as well as 38m and 800m), most of the backscatter obtained at that measurement (focus) height comes from the fog/cloud at low height, where the wind speed is normally lower than that at the measurement height.
  - Additionally, the cloud removal algorithm may interpret that the spectra need to be cloud corrected at the measurement height. If values of the “Cloud Scaling” parameter close to unity are an indication that the data have been cloud corrected, Figure 10 shows that it is the case for most of the datasets with large negative errors.

In case 2:

- The datasets with big positive errors correspond to low values of  $S_{800}$  and high values of  $S_{38}/S_{800}$ , which would indicate the presence of a cloud, and consequently the application of the cloud correction algorithm.
- However, the Cloud Scaling of such points (Figure 10) is between 0.2 and 0.6. It remains unclear whether the cloud correction algorithm was effectively applied to those measurements.

In conclusion,  $S_{800} > 25$  is chosen as an additional filtering criteria, because as seen from Figure 9, it removes from the dataset most of the data with the largest (positive and negative) errors. The effect of applying this filter is shown Figure 11 which depicts the linear regression between the lidar and cup horizontal wind speeds prior to and after applying the  $S_{800} > 25$  filter:

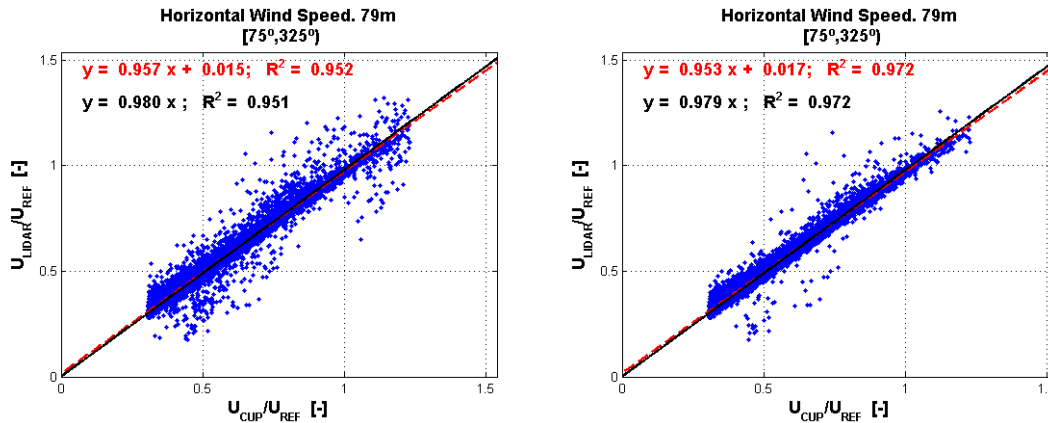


**Figure 11:** 10-minute average values of the horizontal wind speed measured by the lidar and the cup anemometer. Left: without the  $S_{800}$  filter (only filter#1 and filter#2 are applied). Right: after applying  $S_{800} > 25$  (filter#1, filter#2 and filter#3 are applied).

As seen in previous figure, it is not an optimal filter since it doesn't totally remove the data which were suspected of cloud or fog contamination. However it helps in mitigating the effects of fog and low clouds.

#### 4.4 Filter #4: "Turbulence" parameter

Figure 12 presents  $U_{LIDAR} - U_{CUP}$  versus the so-called "Turbulence Parameter". Note that it is not the value of "Turbulence Intensity" commonly defined as  $TI = U_{STD}/U_{MEAN}$  (being  $U_{MEAN}$  the mean value of the horizontal wind speed measured in each ten-minute interval and  $U_{STD}$  the standard deviation). The ZephIR "Turbulence parameter", also known as "Spatial variation parameter" is the turbulence intensity of the radial wind speeds within the circle of scan [8]. Thus, it may be interpreted as an indicator of the goodness of the fit of the radial wind speed measurements in each height scan to the rectified cosine function from which the wind vector is derived. Then, it can be used to filter out data in situations where the wind is not uniform and presents big variations within the lidar circle of scan, at a given height.

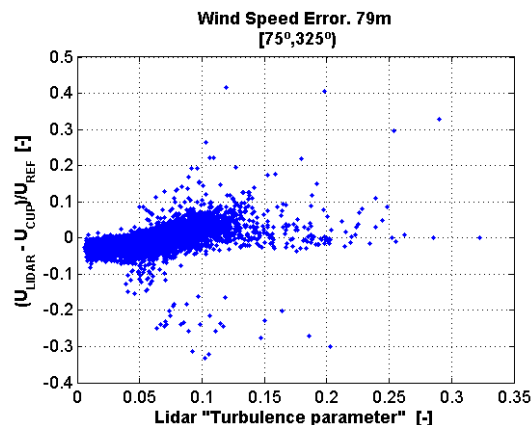


**Figure 12:** (Left) Variation of the wind speed difference with respect to the "Turbulence parameter".

It can be arguable whether this parameter should be used as filtering criteria, since it is to some extent related to turbulence intensity [10], and in filtering data out one would eliminate certain turbulence events. On the other hand, it is also reasonable to think that in the cases of big

(spatial) turbulence, the radial velocities would hardly be well described by the “figure of eight”, and consequently the extracted wind vector would be incorrect. Besides, wrong fits (high “Turbulence Parameter” values) could be caused not only by turbulence but by other reasons such as noise. For this reason, it is chosen as a filtering criteria “Turbulence Parameter” < 0.1.

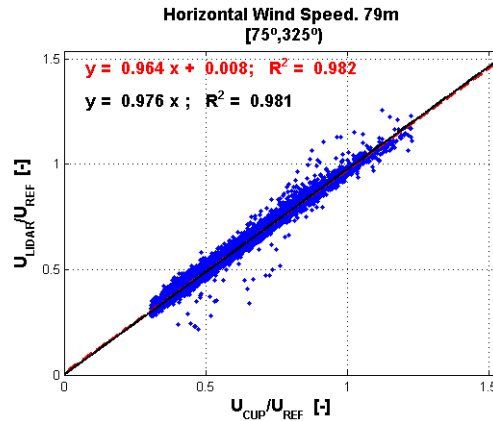


**Figure 13:** Result of applying the filter filter#4 (“Turbulence Parameter” < 0.1) to the dataset in addition to filter#1, filter#2 and filter#3.

Applying further filtering criteria (such as rain, spectral noise, etc) has not shown a significant improvement in data quality (in terms of the regression slopes and  $R^2$  of the previous graph), hence no additional filters are applied.

#### 4.5 Availability of mast and lidar data

The following table summarizes the effect of the previously described filters on the combined availability of mast and lidar data.

Filters	Number of datasets after filtering	% of datasets after filtering
None	16349	100
#1	12685	77.6
#1 AND #2	12406	75.9
#1 AND #2 AND #3	11218	68.6
#1 AND #2 AND #3 AND #4	10497	64.2

**Table 3:** Data availability for different filtering criteria

#### 4.6 Availability and reliability of ZephIR

An Availability and Reliability analysis is performed according to the following definitions, similar to the ones given in [9]. In this section, all the datasets recorded by the ZephIR (including the ones with a “9999” reading) are included. Note that in previous point datasets with simultaneous data from lidar and mast were used, and the ZephIR availability is “hidden” because the different sensors or data acquisition systems have different availability periods.

Here, Availability and Reliability are defined as follows:

“**Availability**” = “number of 10-minute periods during which the lidar was switched on and correctly measuring, divided by total number of 10-minute periods during which it was switched on”

“**Reliability**” = “1 – fraction of time when system was broken or could not be switched on”

For the availability factor calculation, the incorrect data are removed from the dataset recorded by the lidar. This is achieved by applying a series of filters.

Filter	Availability (%)
None	100
Hor_vel≠9999 (Status green or amber)	99.5
Hor_vel≠9999 (Status green or amber) and PIF>=35 and Packets>=50	94.2
Hor_vel≠9999 (Status green or amber) and PIF>=35 and Packets>=50 and Scaling800>25 (fog/cloud filter)	85.9
Hor_vel≠9999 (Status green or amber) and PIF>=35 and Packets>=50 and Scaling800>25 (fog/cloud filter) and “Turbulence”<0.1	79.7

**Table 4:** Lidar availability for different filtering criteria

During this 7-month period the system was not broken. In all the events during which a mains supply cut occurred, the system started functioning on batteries. In the cases when the batteries reached a low level before the mains was restored, the lidar was switched off automatically and had to be turned on manually. No problem or unusual behaviour was observed during the manual start-ups. However, the fact that the system cannot start-up by itself, and the relative difficulty for personnel to access the site where the lidar was installed, led to the interruption of data acquisition during periods of time up to two or three days.

That means, Reliability=100% during this seven-month period, but only taking into account the periods of time where the ZephIR could not be switched on due to a “unit failure (i.e. electrical or laser failure)”. The data not recorded because the lidar could not be switched on autonomously (after a supply interruption) could be considered, to some extent, a source of “Unreliability”. However, this is not easy to quantify (consequently it is not included in the availability or reliability factor calculation).

These are the best availability and reliability results achieved by CENER with ZephIR unit 104 during this lidar’s lifetime up to date (July 2007- February 2011). Although other long-term measurement campaigns were carried out prior to or after this one, this seven-month period without any major unit failures has not been bettered. Besides, the availability factor due to fog has been observed to considerably decrease in other site locations where low clouds and fog are more usual than in the current southern Spain site subject of this study.

## 5. Analysis of Results

The dataset used in the following analysis is the one resulting of the application of all the filtering criteria described in 4.

### 5.1.1 Mean horizontal wind speed analysis

#### 5.1.1.1 Wind speed error distribution

Figure 14 (left) shows the wind speed comparison between lidar and the top-mounted cup (79m height). The linear regressions, performed using two different linear models ( $y=Ax+B$  and  $y=A'x$ ) show an overall underestimation of the wind speed by the lidar. Two group of outlier points are present at high wind speeds and at low wind speeds (likely due to the effect of clouds and fog respectively, not effectively removed by filter#3), where  $U_{LIDAR}$  is noticeably higher or lower than  $U_{CUP}$  in each case. In addition, the plot presents a significant scatter. This is confirmed by the histogram of the error distribution ( $U_{LIDAR} - U_{CUP}$ ), which indicates a negative mean error, however the standard deviation of the error is of the same order of magnitude, as a consequence of the mentioned scatter.

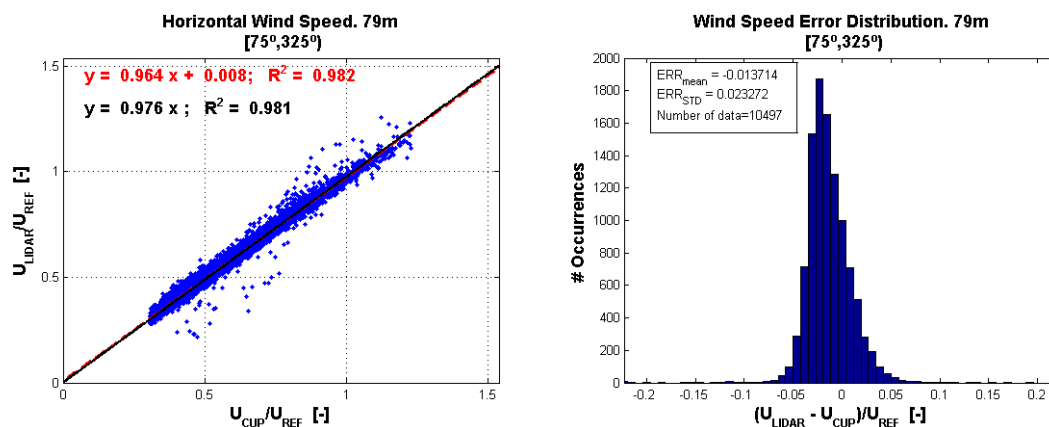


**Figure 14:** Left: lidar to cup wind speed comparison at 79m. Right: histogram of the (normalized) error distribution.

#### 5.1.1.2 Wind speed error and wind direction

One of the main assumptions on which the lidar measurement principle relies, is that wind flow is uniform within the lidar's scan volume [8]. In a site of these characteristics, that is unlikely to be the case, since wind flow curvature is expected to happen due to the complexity of the topography. In addition, from Figure 3 we can see that, since the wind approaching the lidar experiences different changes in orography depending on wind direction, it is expected that the degree of non-uniformity of the wind flow within the lidar's scan volume (and consequently the wind speed error) changes with wind direction. This is checked by plotting  $(U_{LIDAR} - U_{CUP})$  vs wind direction:

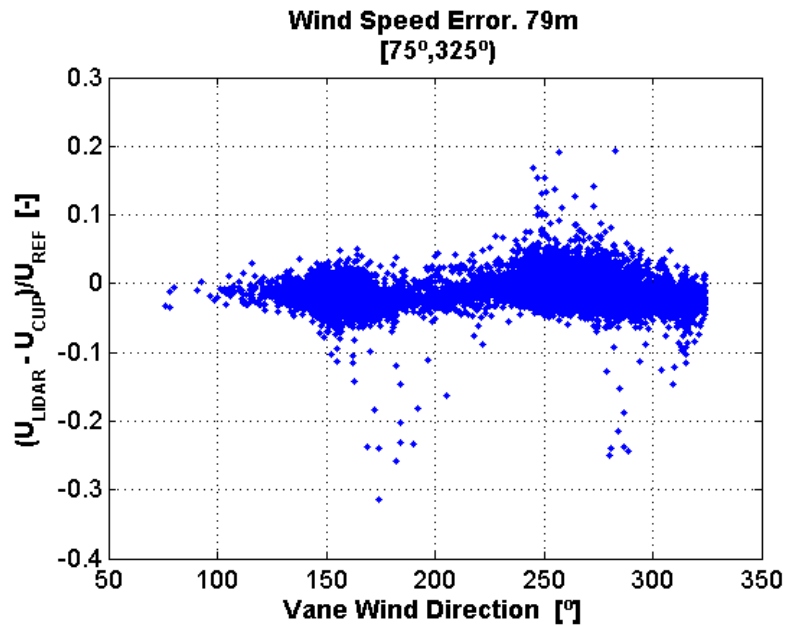


**Figure 15:** Lidar wind speed error (expressed as  $U_{LIDAR} - U_{CUP}$ ) vs wind direction.

In order to better quantify the effect of wind direction (and consequently terrain influence) on lidar wind speed measurements, the dataset is divided in different groups according to wind direction sectors of  $10^\circ$  width within the free sector. For each group, the correlation between lidar and cup measurements is estimated using the two linear regression models previously mentioned ( $y=Ax+B$  and  $y=A'x$ ), and the mean value and standard deviation of  $U_{LIDAR}/U_{CUP}$  is calculated per each direction sector.

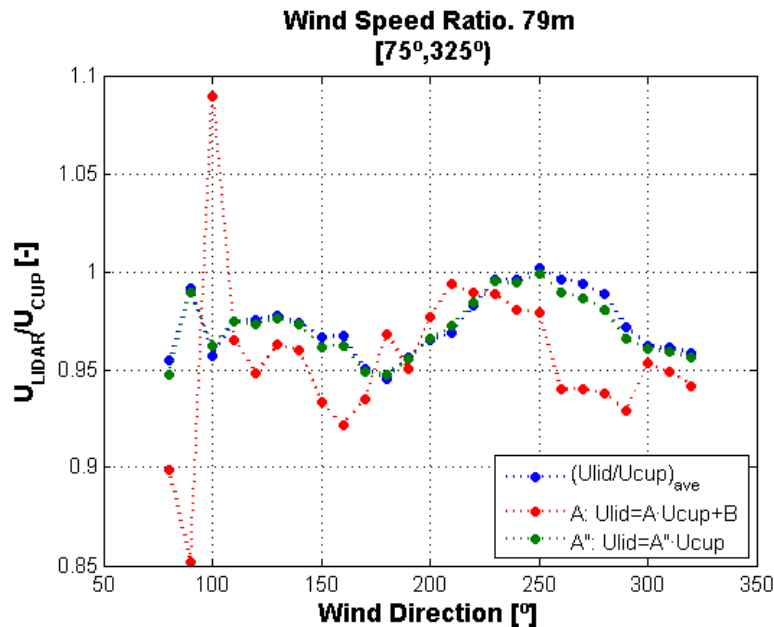


**Figure 16:** Evolution of the slopes of the two regression lines, and mean wind speed ratio, with respect to wind direction.

For the sake of clarity and simplicity, instead of the linear regression parameters, the mean and standard deviation of the lidar to cup wind speed ratio are chosen to illustrate the discrepancy between lidar and cup speeds as a function of direction:

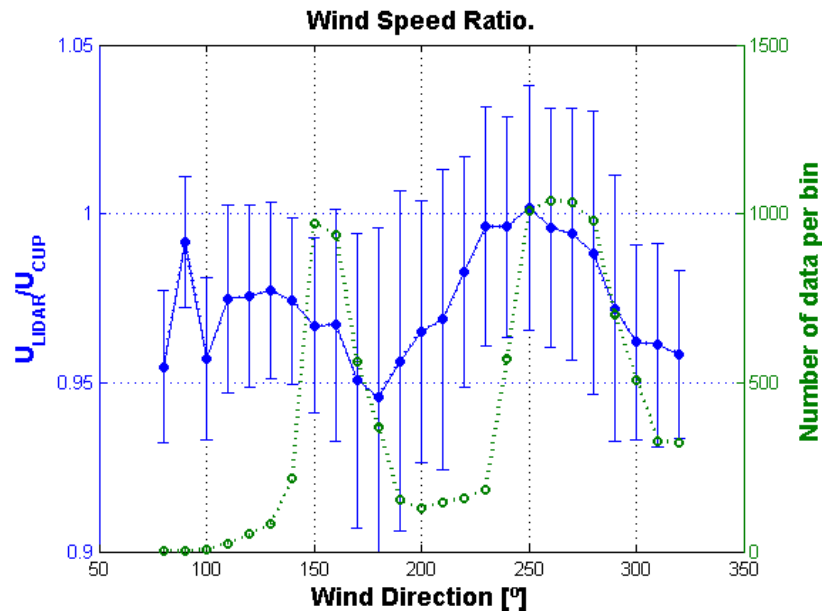


**Figure 17:** Mean wind speed ratio ( $U_{LIDAR}/U_{CUP}$ ) at 79m vs wind direction (blue) and number of data per wind direction sector (green). Error bars represent one standard deviation of the ratio.

### 5.1.1.3 Wind speed error and height

The lidar wind speed measurements at four different heights are compared to the sonic wind speeds in Figure 18. In this case, since sonics are mounted on booms, the measurement sector is reduced, as a first step, to narrower sectors mentioned in 4.1:  $[85^\circ, 125^\circ)$  and  $[265^\circ, 305^\circ)$ , in order to minimize flow distortion effects originated by the mast. However, as seen in Figure 17, the number of data in each  $10^\circ$  sector within  $[85^\circ, 125^\circ)$  is too small to draw representative conclusions, so this sector is not included in the following analysis.

Similarly to Figure 14, the lidar underestimates wind speeds with respect to sonics, in all heights, as seen in Figure 18, which shows that the slope of all regression lines is smaller than unity. However there is not a clear trend in the dependence of the regression slope with height. On the other hand, the histograms (Figure 19) show a broadening of the error distribution with height.

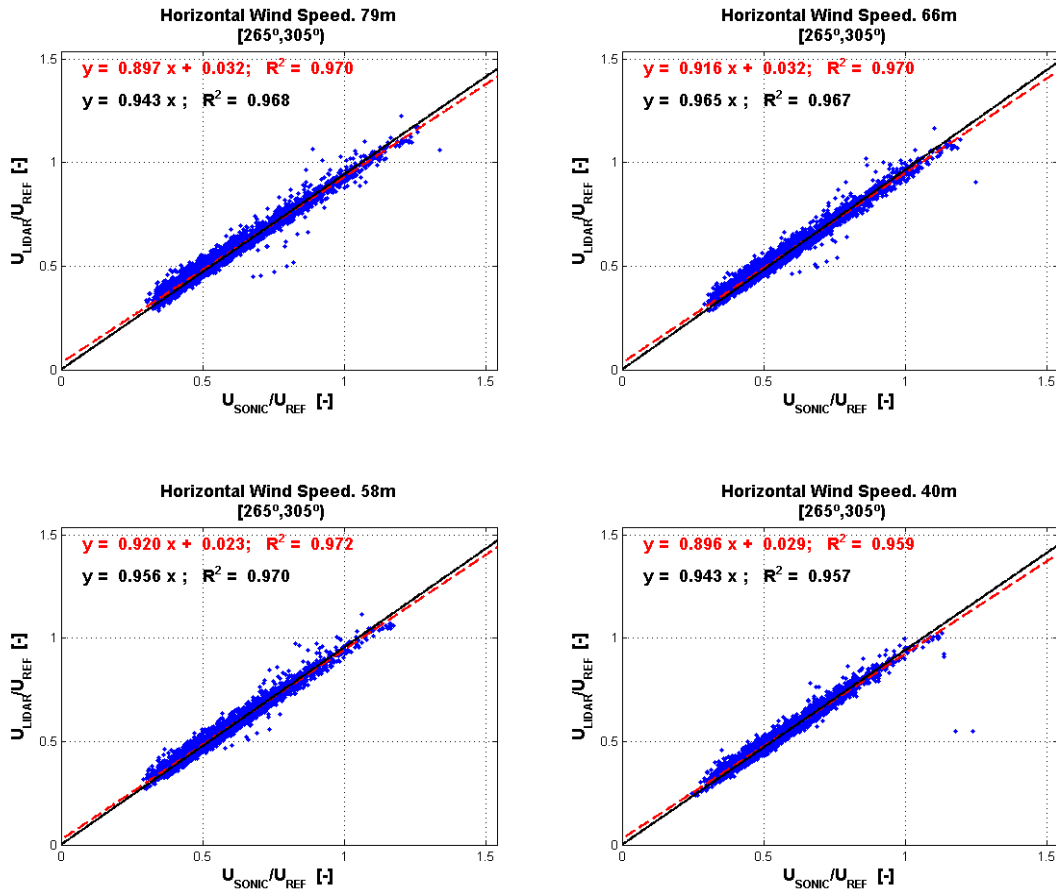


Figure 18: Lidar to sonic wind speed regressions at different heights.

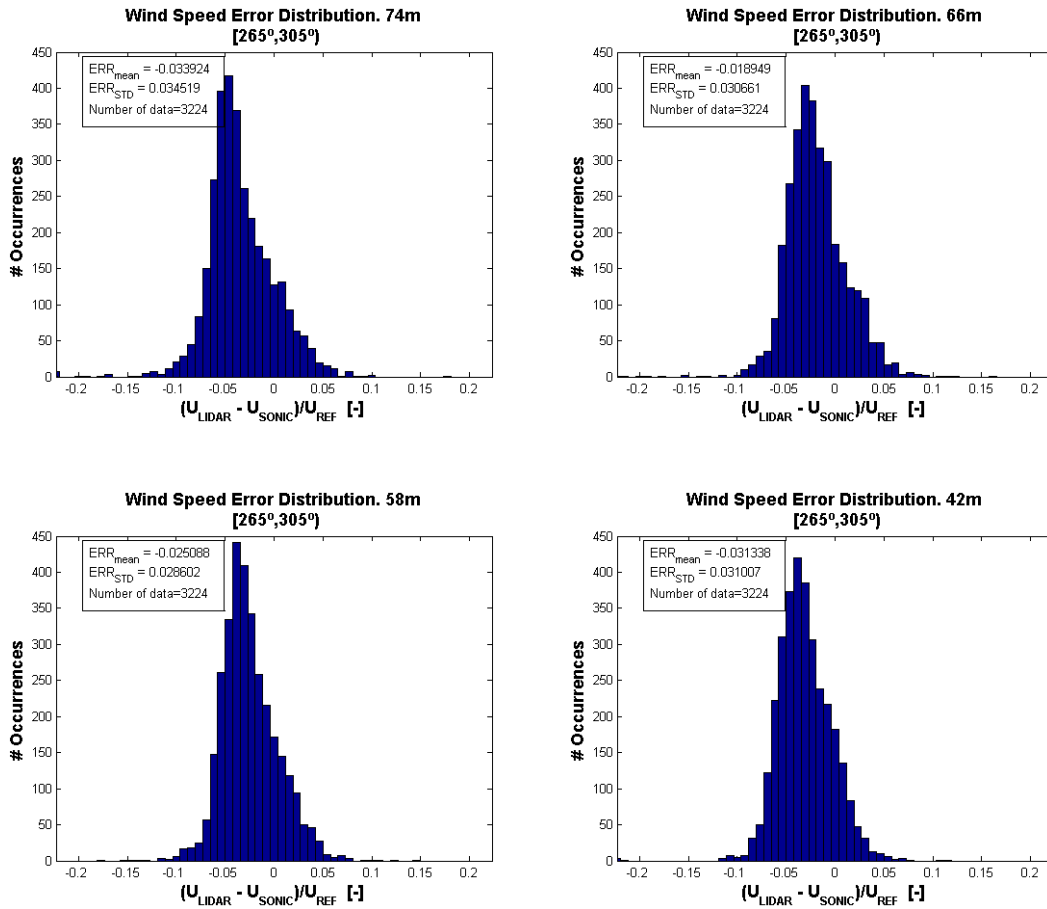
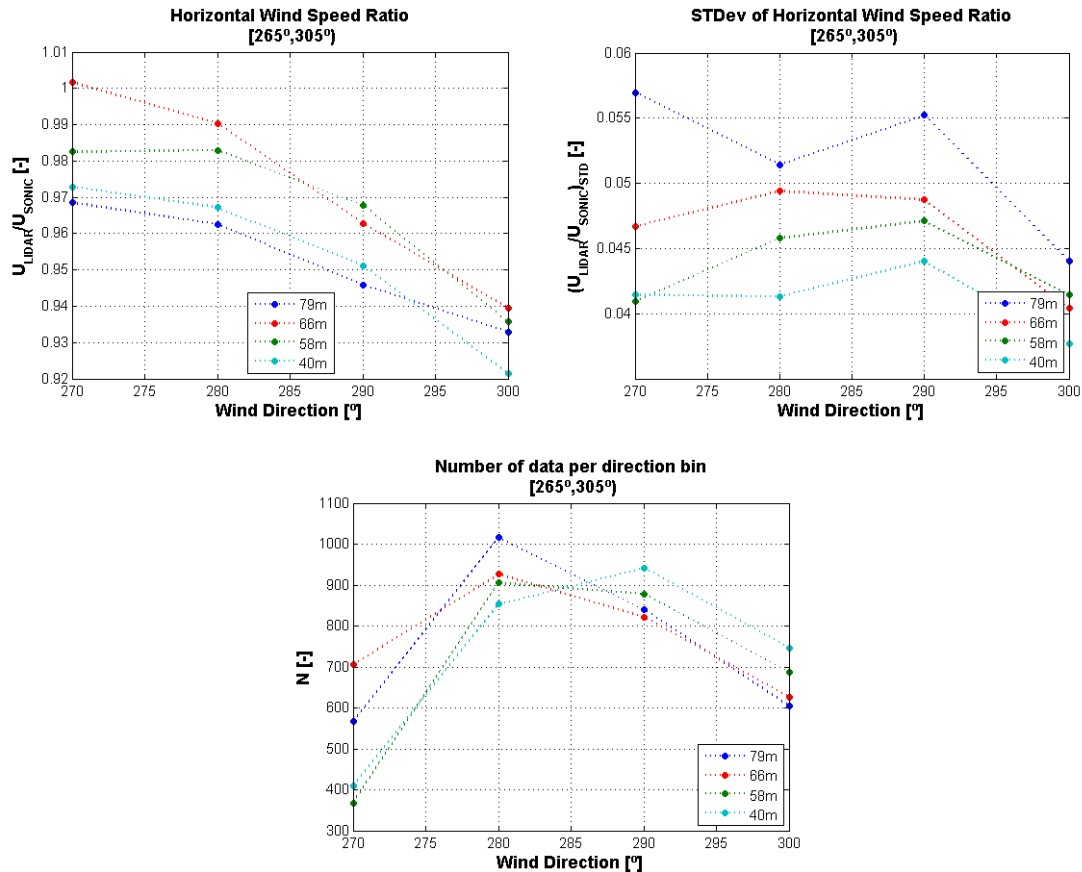


Figure 19: Distribution of lidar wind speed error ( $U_{LIDAR} - U_{SONIC}$ ) at different heights.

A detailed direction analysis, similar to 5.1.1.2 (Figure 17), is carried out at each height, by dividing the  $[265^\circ, 305^\circ]$  sector into  $10^\circ$  sectors and calculating the mean wind speed ratio and its standard deviation per sector and height. Figure 20 (upper left) shows that, as happened with the cup at 79m, the wind speed ratio decreases (for all four heights) as wind direction changes from  $270^\circ$  to  $300^\circ$ . The differences in  $U_{\text{LIDAR}}/U_{\text{CUP}}$  between the different heights can be considered negligible, since those differences lie within the uncertainty of the mean, given the standard deviations plotted in Figure 20 (upper right). The standard deviation of the wind speed ratio increases with height, in all sectors. This is probably due to the increase of the lidar probe volume with height [8] and a greater sensitivity to clouds.



**Figure 20:** Top Left: Mean of the ratio between lidar and sonic wind speed, per direction bin. Top Right: Standard deviation of the ratio between lidar and sonic wind speed, per direction bin. Bottom: Number of data per direction bin.

#### 5.1.1.4 Wind speed error and wind speed

When plotted as a function of wind speed (Figure 21) it can be seen that the lidar error displays, to some extent, a linear dependency with wind speed (cup speed). For a lidar scanning a uniform wind flow ( $U$ ), an error in cone angle ( $\Delta\phi$ ) implies an error in the wind speed measured by the lidar directly proportional to the wind speed:  $\text{error} = k \cdot U$  (where  $k$  is a constant) [11]. Consequently, in this measurement campaign a cone angle error might not be excluded. However, in this case it is difficult to separate the possible error due to cone angle from other sources of error (such as the dependency with direction – terrain –, as seen in 5.1.1.2).

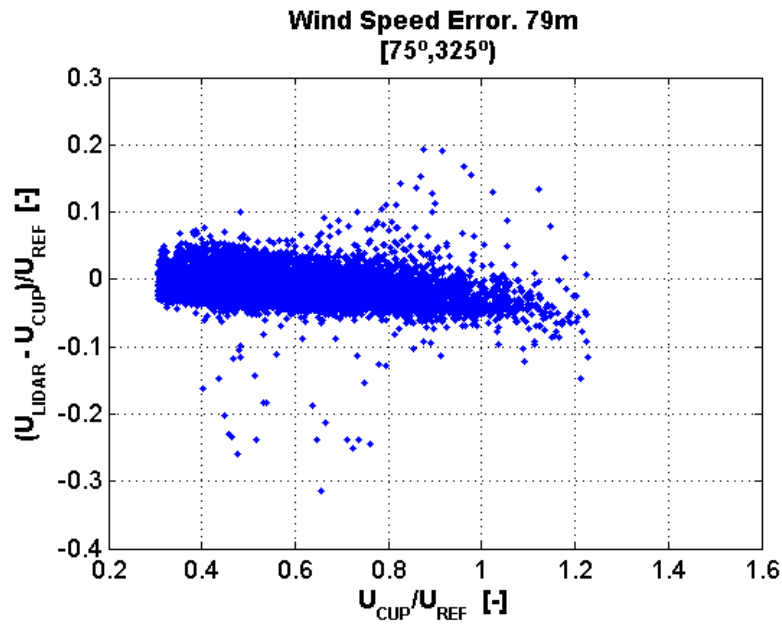


**Figure 21:** Lidar error versus cup wind speed at 79m.

Although cone angle is carefully measured by the manufacturer during calibration [12], an incorrect lidar deployment (i.e. tilted lidar) would increase the negative impact of a small cone angle error. During installation, the ZephIR lidar is normally levelled by means of a spirit level during assembly of the pods. It would help reduce the uncertainty due to mounting if the lidar included an internal sensor of the tilt of the optic component.

#### 5.1.1.5 Wind speed error and wind flow angle

Next figure depicts the difference between lidar wind speed and sonic wind speed as a function of the wind flow angle (tilt), at different heights. The four heights present a similar trend, but the scatter of each group increases with height (which is in accordance to 5.1.1.3).

The four data sets present a significant spread for negative angles, which tends to narrow as the tilt angle increases. In principle, wind flow tilt would not induce an error in the lidar measurement as long as the wind inclination angle is fairly constant throughout the lidar scan volume. A change in wind tilt within the scanning volume would cause errors, since it would violate the assumption of uniform wind within the scan volume on which the lidar measurement principle is based.

In a later section we will analyse the dependence of tilt with direction.

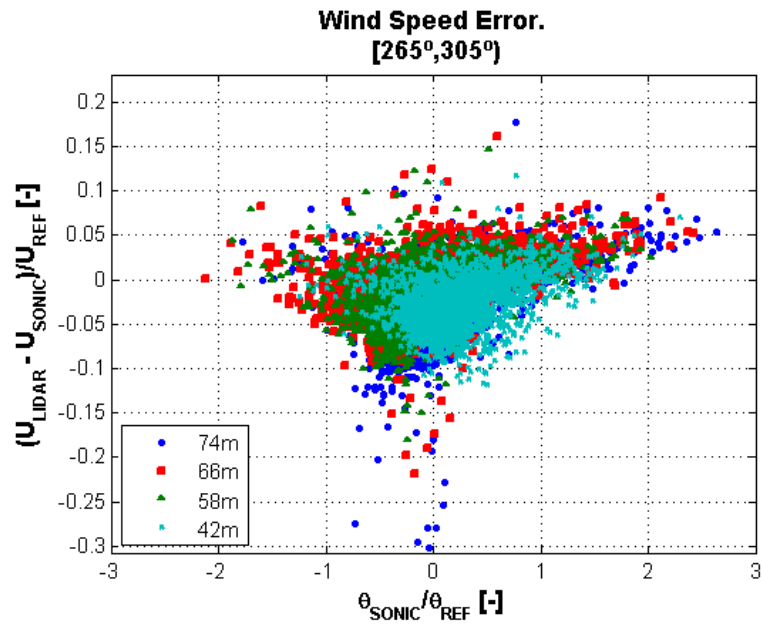


Figure 22: Lidar error ( $U_{LIDAR} - U_{SONIC}$ ) vs sonic tilt angle at different heights.

5.1.1.6 Wind speed error and shear

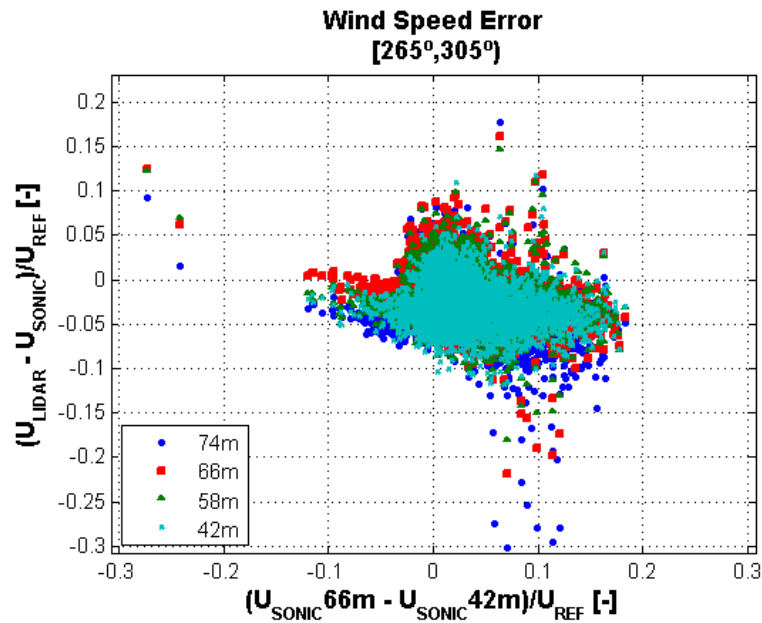


Figure 23

Figure 24: Lidar wind speed error ( $U_{LIDAR} - U_{SONIC}$ ) vs wind shear (defined as  $U_{sonic\_66m} - U_{sonic\_42m}$ )

As in previous case, the four heights present a similar pattern for the evolution of  $U_{LIDAR} - U_{SONIC}$  with wind shear. Here, for simplification shear is defined as  $\Delta U = U_{SONIC\_66m} - U_{SONIC\_42m}$  (the wind speed difference between the sonic at 66m and the sonic at 42m). This plot shows how different an effect shear has in this case when compared to flat terrain conditions [11].

For negative shear values,  $U_{LIDAR} - U_{SONIC}$  follows a descending trend as  $\Delta U$  approaches zero. When  $\Delta U$  takes values close to zero (vertical profile close to being flat) there is surprisingly a big scatter around  $U_{LIDAR} - U_{SONIC} = 0$ . This should be the most favourable case (i.e. lowest error due to shear), since the wind speed would be close to constant along the lidar probe length at each point of the scan. For values of  $\Delta U > 0$ , error tends to narrow down towards a negative value.

#### 5.1.1.7 Wind speed error and veer

No clear dependence is observed between the wind speed difference between lidar and cup on wind veer:

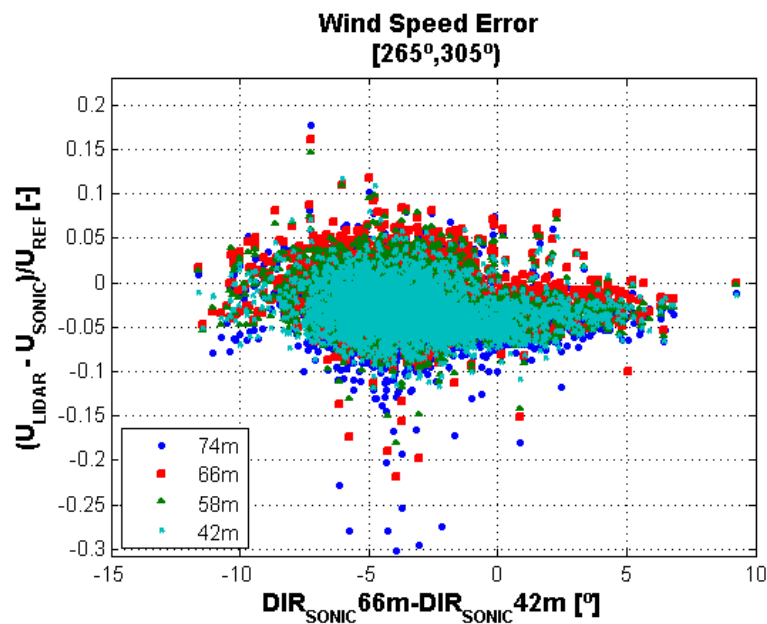


**Figure 25:** Lidar wind speed error ( $U_{LIDAR} - U_{SONIC}$ ) vs wind shear (defined as  $U_{sonic\_66m} - U_{sonic\_42m}$ ) at different heights

#### 5.1.1.8 Wind speed error and turbulence

Considering turbulence in terms of the standard deviation of the cup wind speed, next figure shows that there is not a clear dependence between the lidar wind speed error and the cup turbulence. The wind speed difference  $U_{LIDAR} - U_{CUP}$  remains practically constant with  $\sigma_{U_{cup}}$ .

Once again, it has to be remembered that the cup makes a point measurement, whereas the lidar makes a volume measurement. At sight of Figure 26 and Figure 12, the lidar wind speed error is more influenced by the differences in turbulence between the points of scan (the bigger the difference, the bigger the "Turbulence Parameter"), than by the level turbulence at a given reference point (cup measurement).

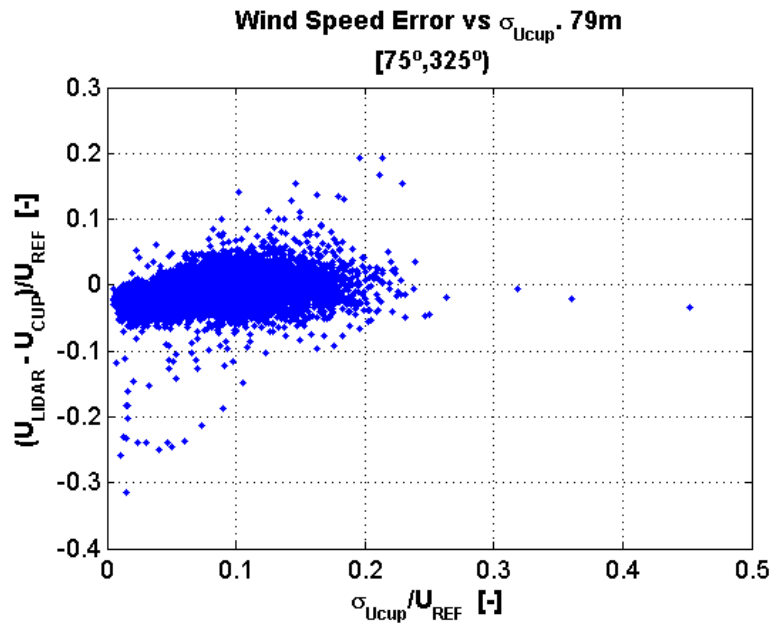


**Figure 26:** Lidar wind speed minus cup wind speed plotted vs the standard deviation of the cup wind speed.

### 5.1.2 Wind direction analysis

The wind direction measured by the lidar at different heights has been compared to the wind direction provided by sonics and wind vanes distributed along the mast. In general, a very good agreement is found between the lidar and the mast instruments. For the sake of brevity, only the comparison with the vane at 77m height is shown in next figure.

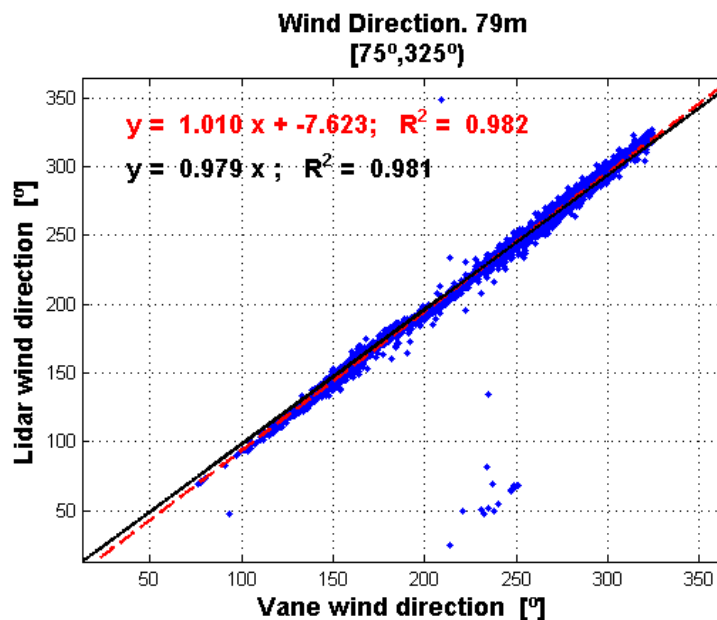


**Figure 27:** Lidar wind direction plotted vs vane direction

The correlation between lidar and vane is very good, with two minor exceptions. One is a “bump” in the linear distribution around 180° wind direction, which is likely due to the vane being affected

by the mast wake in that direction (boom orientation indicated in Table 1). Second, there is a small group of data for which the lidar presents a  $180^\circ$  error in the direction value. It is likely due to an incorrect estimation of the wind sense in cases of strong wind veer. It has to be remembered that by the ZephIR measurement principle, it has a  $180^\circ$  ambiguity in resolving the wind direction, which is resolved by a vane in its meteorological mast that is approximately 2m a.g.l – thus the  $180^\circ$  error when there is significant wind veer.

### 5.1.3 Vertical wind speed analysis – Rain influence

Comparing the vertical wind speed measured by the lidar to that measured by a propeller (Figure 28) or a sonic anemometer (Figure 29), two things are observed:

- Rain produces big errors in the vertical speed measured by the lidar.
- The data obtained in dry conditions show that the lidar vertical wind speed and the propeller or sonic vertical wind speed have a lineal dependence. However, the slope of the linear trend is smaller than unity. This means: lidar underestimates the magnitude of the vertical wind speed.

The second point could be explained by the lidar performing an averaging of the vertical wind speeds of all the points of scan, which in a complex terrain of this characteristics is expected to change significantly (compared to the magnitude of the speed) along the points of scan.

In the comparison to the propeller the linear dependence between the lidar and the anemometer is distorted by a group of points between  $0.05U_{REF}$  and  $0.1U_{REF}$ . The origin of this has not been found.

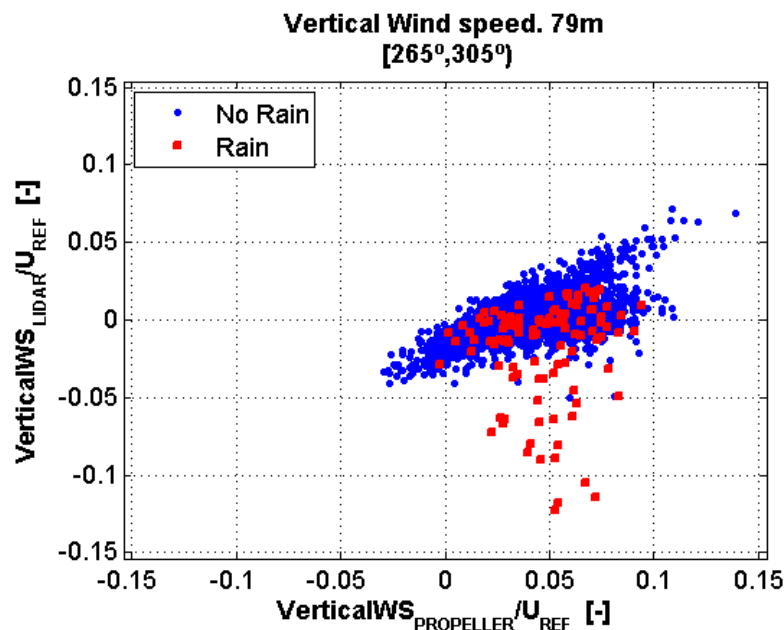


**Figure 28:** Comparison of vertical wind speed measured by the lidar and the propeller. Datasets corresponding to rainy conditions are marked in red.

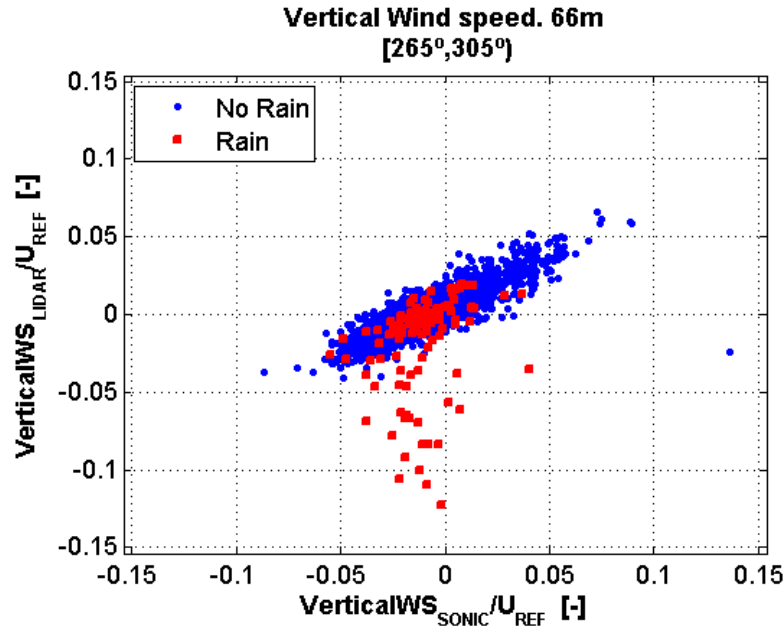


**Figure 29:** Comparison of vertical wind speed measured by the lidar and the sonic. Datasets corresponding to rainy conditions are marked in red.

#### 5.1.4 Wind flow angle analysis

Due to the observed negative impact of rain in the vertical wind speed measured by the lidar in the previous point, the following analysis is done for dry conditions (data is additionally filtered for Rain=0).

When comparing the tilt measured by the lidar and the sonic anemometers at different heights (Figure 30), a linear trend is observed once again (it happened too in the analysis of horizontal and vertical speeds, and logically it is translated to tilt angle), at all heights. Due to the lidar severe underestimation of the vertical speed, the tilt angle is also underestimated (slopes of linear trends in Figure 30 smaller than one).

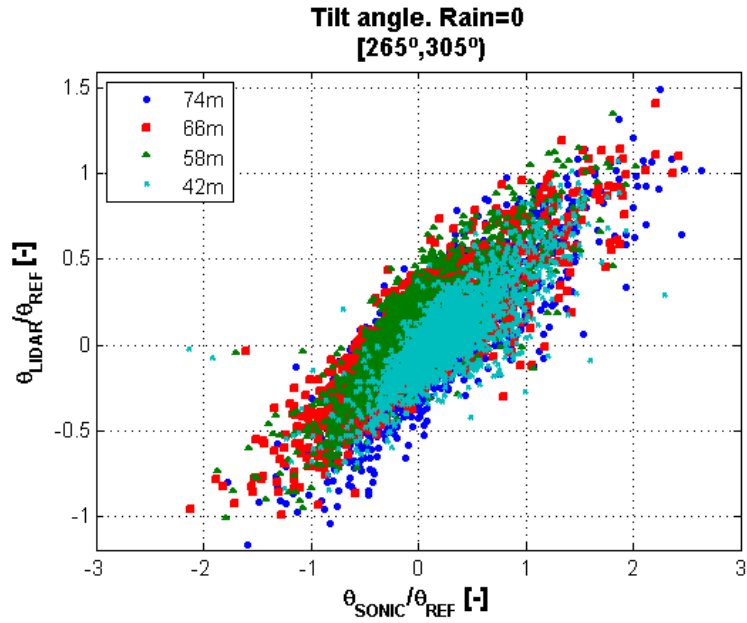


**Figure 30:** Tilt measured by lidar compared to tilt measured by sonic at different heights

However, even if the tilt measured by the lidar is smaller than the one measured by the sonics, it follows approximately the same tendency with wind speed (Figure 31 and Figure 32) and wind direction (Figure 33).

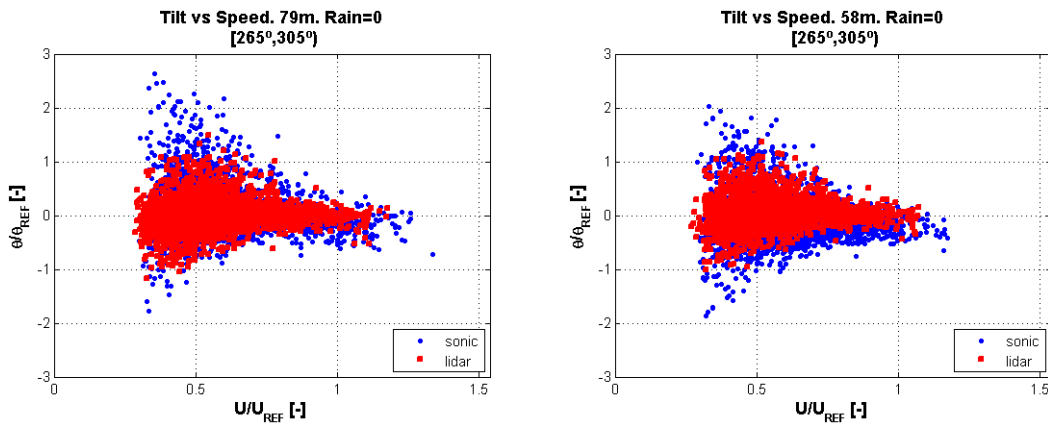


**Figure 31:** Evolution of tilt angle with respect to wind speed, measured by the sonic (blue) and the lidar (red) at 79m (left) and 40m (right).

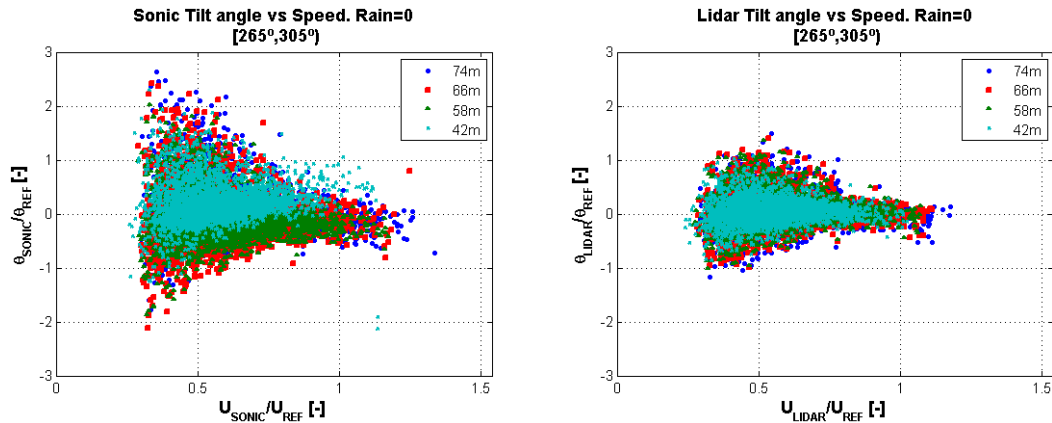


**Figure 32:** Evolution of tilt angle with respect to wind speed, at for heights, as measured by the sonics (left) and the lidar (right).

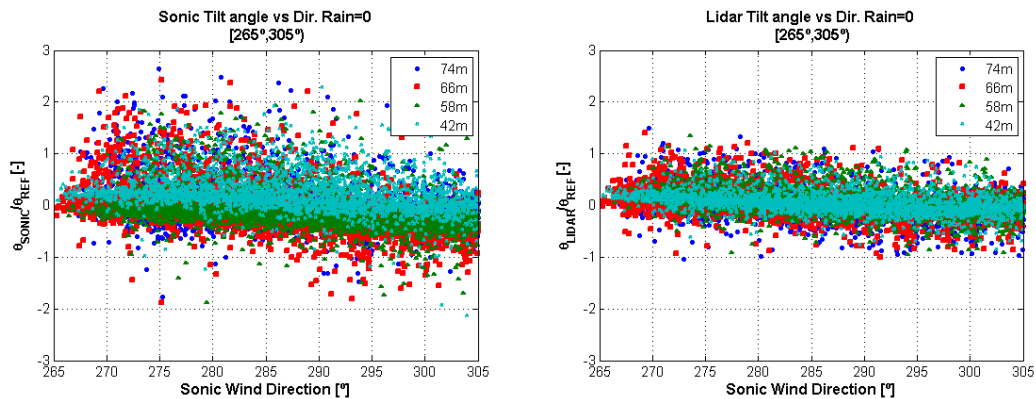


**Figure 33:** Tilt angle with respect to wind direction, at for heights, as measured by the sonics (left) and the lidar (right).

### 5.1.5 Turbulence analysis

Finally, the turbulence measured by the lidar is compared to the turbulence measured by the cup anemometers. Turbulence is understood here as the standard deviation of the horizontal wind speed ( $\sigma_U$ ), instead of the usual “Turbulence Intensity”,  $TI = \sigma_U / \text{mean}(U)$ . This is done because, as seen in previous sections, the lidar tends to underestimate the cup speed, thus using the common TI definition may end up in misleading results.

Figure 34 shows that the standard deviation measured by the lidar follows a similar tendency with respect to wind speed and wind direction as the standard deviation measured by the cup. It is observed in both plots that the lidar  $\sigma_U$  is somewhat smaller than the cup  $\sigma_U$ . This is underestimation is quantified in Figure 35, which presents the comparison of  $\sigma_U$  of lidar and cup at two different heights (79m and 40m).

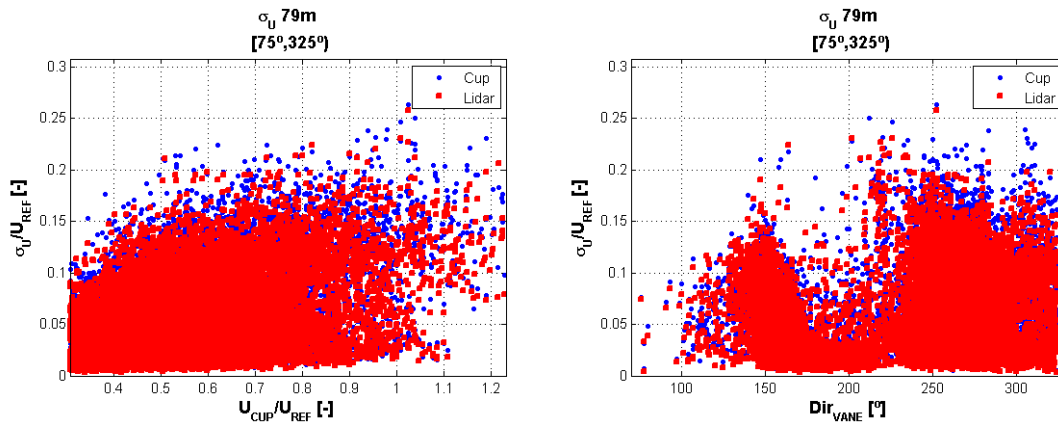


**Figure 34:** Standard deviation of the horizontal wind speed as measured by the cup anemometer (blue) and the lidar at 79m, plotted vs wind speed (left) and wind direction (right).

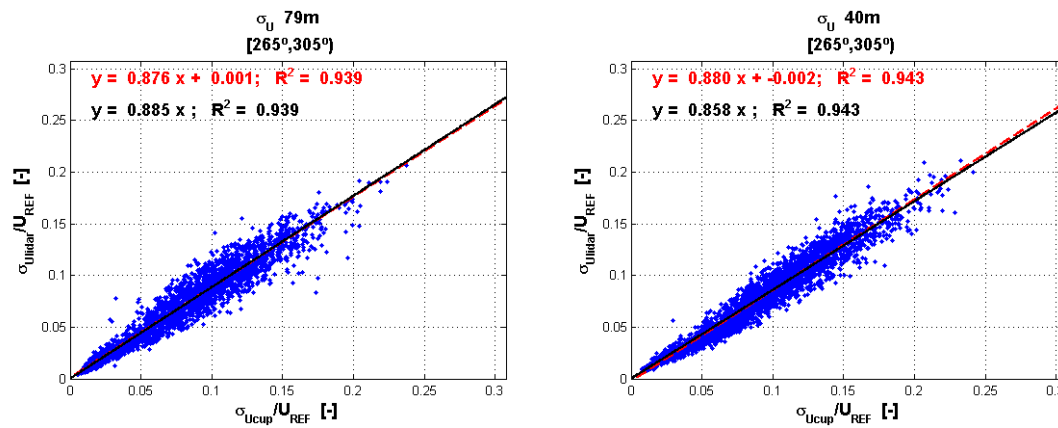


**Figure 35:** Standard deviation of the horizontal wind speed measured by the lidar versus standard deviation of the horizontal wind speed measured by the cup anemometer at 79m (left) and 40m (right)

The first observation from Figure 35 is that, although the linear dependence between the cup standard deviation and the lidar standard deviation is clear in both heights, they are not so well correlated (i.e.  $R^2$  is lower) as the wind speeds were (5.1.1). The second observation is the slopes of the regression lines are in both cases smaller than one. This means, the lidar is underestimating turbulence. This is explained in [10] as the result of the spatial averaging performed by the lidar (both along the radial directions, in each probe volume; and along the circle described in each scan). The result of that spatial averaging is that the lidar cannot measure turbulence structures that are of orders of magnitude smaller than the lidar circles of scan.

However, the theoretical model and the flat terrain results in [10] show that in average the wind speed standard deviation measured by the lidar is 0.8 times the wind speed standard deviation measured by the cup. In our case, it is higher (0.88 at 79m and 0.86 at 40m), probably due to some contribution from the  $\sigma_w$  from the (real) wind to the  $\sigma_U$  measured by the lidar. This is in line with other to other complex terrain results from WP6 [13].

## 6. Modelling lidar measurements

A Wasp Engineering script has been developed by Risø-DTU to model lidar measurements and to predict direction dependent wind speed errors of a lidar in a given terrain [14]. Summarizing, the Wasp code simulates (for a set of directions defined by the user):

- The radial velocities along the lidar laser beam directions, of each circle scan at each measurement height. Then, the wind vector is derived from the radial velocities, performing the same fitting routine as the lidar does.
- The wind vector in all measurement heights at the lidar position, or at any other position (i.e “reference” position) on the given terrain.

Once both vectors have been derived, for each given wind direction and each height, the ratio between the lidar horizontal wind speed and the wind speed at the reference position is calculated. This tool models both ZephIR and WindCube lidars.

Figure 36 presents an example of the typical ZephIR conical scan geometry, and the points of scan and radial wind speed vectors in those points, simulated by the WaspEng script.

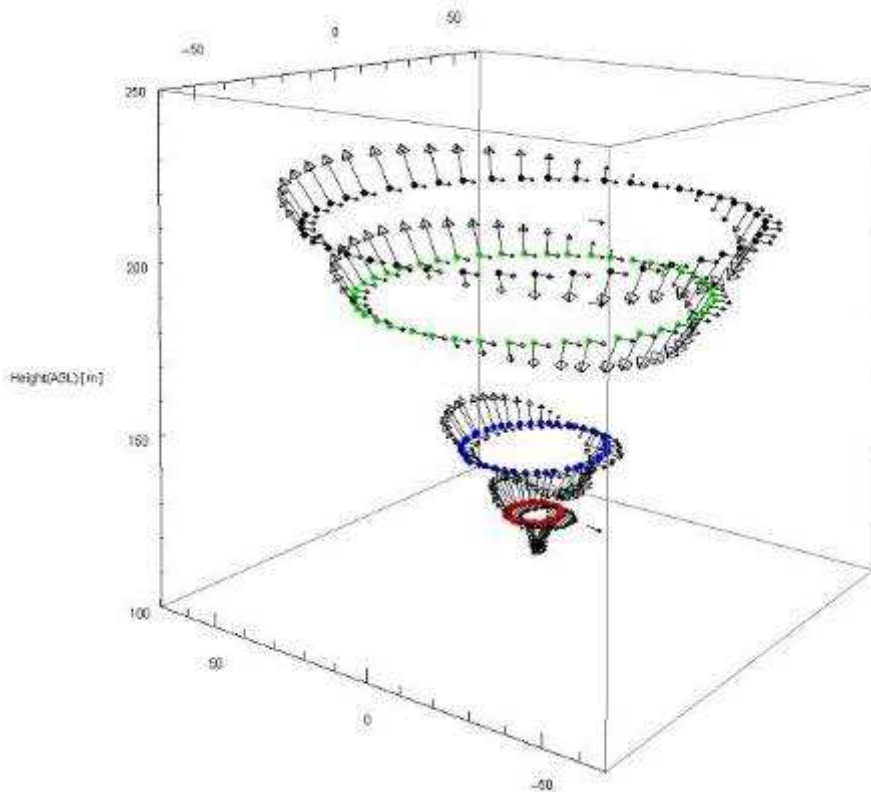


**Figure 36:** Example of radial projections of simulated wind vectors at the points of scan of a ZephIR. Reproduced from [15]

A similar approach has been followed too by lidar manufacturers, but using CFD codes instead of WaspEng to perform the modelling, with very positive results in complex terrain [17] [18].

From the results obtained in this measurement campaign in complex terrain (Figure 17), there is a clear dependence of the lidar wind speed underestimation as a function of wind direction. This

presents a very good opportunity to check to what extent both modelling approaches (with both linear and not linear codes) can be useful to predict lidar wind speed errors in complex terrain.

In this section, the Wasp lidar script is first used to produce horizontal wind speed ratios between the lidar and the nearby mast ( $U_{\text{LIDAR}}/U_{\text{CUP}}$ ) for a group of wind directions bins within the valid measurement sector. Secondly, CENER's CFD code, CFDWind 2.0, has been applied too to this case with the same purpose.

## 6.1 Wasp Engineering lidar Script

The main configuration parameters of the script were set as follows:

- The same coordinate was introduced for lidar and mast. In the experimental set-up the lidar is located very close to the mast (12m), which can be considered negligible with respect to map resolution and the diameters of the circles of scan at the heights of interest.
- Setting the heights to be simulated to match lidar measurement heights
- Cone angle of this particular unit.

The script was executed for different definitions of the wind direction bins:  $1^\circ$ ,  $5^\circ$  and  $10^\circ$ . All of them produced very similar results. The result presented in 6.3 corresponds to the ( $U_{\text{LIDAR}}/U_{\text{CUP}}$ ) ratio obtained with the  $5^\circ$  direction bin configuration at 79m.

## 6.2 CFD modelling

### 6.2.1 Description of CFDWind 2.0

The non-linear CFD code CFDWind 2.0 [16] developed by CENER is based on the commercial software package FLUENT 12.0. A specific adaptation of Fluent has been made for the simulation of the mean wind components and turbulence intensity in the atmospheric boundary layer. The code is particularly focused on the simulation of wind in complex terrain, although it can be applied to many other environments. Air is considered as an incompressible fluid.

CFDWind 2.0 solves elliptically the Navier Stokes equations: conservation of mass, momentum and energy in the atmospheric boundary layer, taking into account thermal effects for the simulation of non-neutral atmospheres as well as the Coriolis force. Turbulent closure is based on a modified k-eps model, from the Apsley and Castro theory for the limitation of the length scale. Buoyancy effects are activated when non-neutral atmosphere is to be modelled.

The code can work with different types of mesh geometries, although structured grids are mostly used from the commercial mesh generator ICEM CFD 11.0. Inlet boundary conditions are based on the profiles of wind speed components, turbulent kinetic energy and turbulent dissipation rate from a previous 1D simulation of the fully developed turbulent boundary layer. The ground is simulated through the standard wall functions modified for roughness and parameterized according to local aerodynamic roughness length and wall heat flux. Pressure outlet is the most frequently used one at the outflow boundary condition.

Stationary approximation is the most common choice at operational level of the model although transient simulations can also be carried out.

Output data files can be exported in 1D/2D profiles or list of output variables.

## 6.2.2 Set-up

The application of CFDWind2.0 to this case consists of extracting the (u,v,w) velocity components at various points from the lidar conical scan. The influence of possible flow distortion (inside the lidar scan volume and with respect to the meteorological mast position) produced by the terrain variation is thus taken into account by the model.

When applying the procedure it is usually highly recommended to validate the model against a second met mast in the surroundings of the wind farm in order to guarantee the procedure and supply an uncertainty level. However, in this case study no “blind test” of the results was performed. This would be closer to most real life applications of the use of CFD codes to predict lidar errors, where CFD would be used to estimate errors of lidars which are deployed in stand-alone configurations.

The simulation of this lidar deployment with CFDWind2.0 was carried out at the latest stages of the UpWind Project (September-October 2010). Due to the time limitation, and due to the complexity of the preparations and the duration of the CFD simulations, only the predominant wind direction sector [225°,305°) has been simulated, instead of the whole [75°,325°) free measurement sector. It has been considered that this sector is wide enough and has sufficient amount of experimental data for demonstration purposes.

As in the case of the Wasp simulation, lidar has been assumed to have the same coordinates as the meteorological mast. Analysis is performed for 10°-width direction sectors.

## 6.3 Results

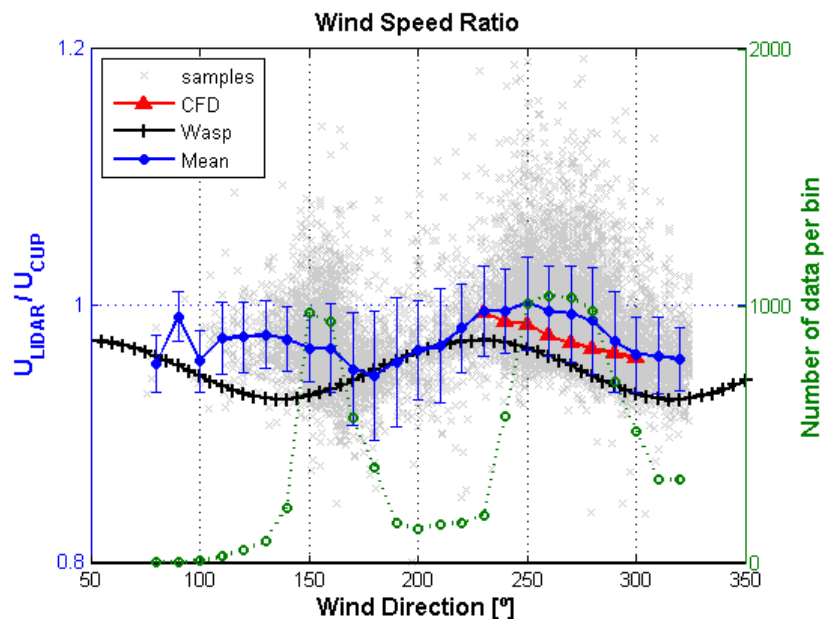


**Figure 37:** Mean lidar wind speed to cup wind speed ratio obtained per wind direction sector by CFD simulations (red), WaspEng simulations (black) and experimental measurements (blue). The error bars represent one standard deviation of the experimental ratio.

It can be seen that the results of both models follow well the tendency, and are within the uncertainty limits, of the experimental results inside the predominant (west) direction sector. However, CFD results are closer to the mean values obtained from the measurements; the

discrepancy between model and measurements is smaller than 2% (which is the maximum difference, found at 280°). Wasp results lie in the boundary of the measurement uncertainty.

In the [165°,225°) sector there is an excellent agreement between WaspEng and experimental results. However such is not the case of the [125°,165°). It is curious to note that the WaspEng  $U_{\text{LIDAR}}/U_{\text{CUP}}$  prediction displays a sinusoidal dependence with direction as seen in the experimental results, however here left-shifted. The reason for this is not clearly understood.

## 7. Conclusions

This report has summarized the results of a measurement campaign with a lidar in complex terrain. This section summarizes the most relevant conclusions drawn from the data analysis.

It's worth pointing out that special emphasis has been put in describing the filtering process and explaining what limits have been chosen and why. It is important to remember that lidar data need to be as carefully checked and filtered as mast data. Even when lidars present less restrictions in terms of mounting effects than mast instruments (such as errors in measurement due to flow distortion from mast or booms, etc), they suffer other type of constraints, such as the effect of fog/clouds.

The main conclusions drawn from the experimental results are:

- A general underestimation of the horizontal wind speed by lidar has been found when compared to cup anemometers and sonics.
- This discrepancy in the horizontal wind speed (or “wind speed error”) has been investigated by comparison with different variables (wind speed, wind direction, inflow angle, etc). Of all them, it has been found that it is wind direction the one that most influences the wind speed error.
- In particular, the wind speed ratio between lidar and cup has been found to change with direction. This is accounted for by the terrain effects.
- The wind direction measured by the lidar has been found to be in very good agreement with the mast instrumentation.
- It has been observed that the lidar in this deployment significantly underestimates the vertical wind speed and consequently the wind inflow angle.
- The analysis of the standard deviations of the horizontal wind speeds confirms that the lidar underestimates turbulence. However, the ratio between lidar and cup standard deviations of the horizontal wind speeds has been found to be bigger than in flat terrain cases.

Additionally, two different tools (Wasp Engineering and CFD) have been used to model the lidar measurement in this particular deployment, in order to check to what extent they can predict the direction-dependent lidar error. Both of them have achieved fairly acceptable results in a given sector of interest. This kind of numerical modeling approaches is very attractive for its combined used with lidar deployments in complex terrains: the flow model could be used to predict the lidar error either for the purpose of correcting lidar measurements, or for choosing the most appropriate location (i.e. the one where the lidar would experience a smaller error) prior to its deployment in the field.

## 8. Acknowledgements

The author would like to express her gratitude to Gustavo Rodríguez and Sogepyme S.A. for allowing this campaign to be carried out and for the assistance provided during it.

This work would have not been possible without the field support of the technicians and the collaboration of the power curve engineers, from the Field Tests area at CENER's Wind Turbine Test Laboratories.

Thanks to: Bibiana García, Elena Cantero and Daniel Cabezón for their contributions to 6.2; to Mike Courtney and Rozenn Wagner for their invaluable collaboration in the campaign deployment; to Mike Harris, Chris Hill and Ferhat Bingöl for their comments and advice.

The previously mentioned persons are not responsible of any possible errors or omissions in this report.

## 9. References

1. P. Gómez "UPWIND D6.15.1 Report – An approach to power curve with lidar in complex terrain". 2011
2. IEC 61400-12-1 "Power performance measurements of electricity producing wind turbines", Edition 2005.
3. UNE-EN ISO/IEC 17025:2000 "Requisitos generales relativos a la competencia de los laboratorios de ensayo y calibración".
4. MEASNET "Cup Anemometer Calibration Procedure Version 2". October 2009.
5. Metek "USA-1 User manual". 2005.
6. T.F. Pedersen, J.-Å. Dahlberg, P. Busche "ACCUWIND – Classification of five anemometers according to IEC61400-12-1". 2006.
7. C. Hill, M. Harris "UPWIND D6.3.1 - QinetiQ Report on cloud removal algorithm". 2010.
8. C. Hill, M. Harris "UPWIND D6.1.1 - QinetiQ lidar measurement report". 2010.
9. C. Hill "UPWIND D6.14.1 - QinetiQ lidar availability report". 2010.
10. R. Wagner, T. Mikkelsen, M. Courtney "Investigation of turbulence measurements with a continuous wave, conically scanning LiDAR". Risø-R-1682(EN). 2009.
11. P. Lindelow "UPWIND D6.1.3 Report - D1. Uncertainties in wind assessment with lidar". 2007.
12. C. Hill "UPWIND D6.2.3 – QinetiQ lidar calibration report". 2010.
13. D. Foussekis "UPWIND D6.6.1 Report. Remote Sensing – CRES activities". 2011
14. F. Bingöl, J. Mann "Lidar performance estimation script for WAsP Engineering". Risø-R-1664(EN). 2008.
15. F. Bingöl, j. Mann, D. Foussekis "LiDAR error estimation with WAsP Engineering". ISARS 2008 proceedings.
16. J. Sanz, D. Cabezón, S. Lozano, I. Martí "Parameterization of the atmospheric boundary layer for offshore wind resource assessment with a limited length-scale k-ε model". EWEC 2009 proceedings.
17. M. Harris, I. Locker, N. Douglas, R. Girault, C. Abiven, O. Brady "Validated adjustment of remote sensing bias in complex terrain using CFD". EWEC 2010 proceedings.
18. M. Boquet, R. Parmentier, L. Sauvage, J.P. Cariou "Theoretical and CFD analysis of pulsed Doppler lidar wind profile measurement process in complex terrain". EWEC 2010 proceedings.